Design and Performance Comparison of Fractional Slot Concentrated Winding Spoke Type Synchronous Motors With Different Slot-Pole Combinations

Enrico Carraro, Nicola Bianchi, *Fellow, IEEE*, Sunny Zhang, and Matthias Koch

***Abstract*—Fractional slot concentrated winding (FSCW) interior permanent magnet (IPM) synchronous motors are nowadays an attractive solution in automotive applications due to their advantages in terms of high performance and manufacturing simplicity. Among the different topologies, the spoke type is an effective configuration when high torque density is required. On the other hand, the motor performance are heavily related to the selected slot-pole combination. This choice is critical in demanding automotive applications, such as electric power steering (EPS) systems, where high constraints in terms of torque density, torque quality, flux weakening performance, and noise/vibration/harshness are requested. This paper deals with the design and analysis of eight optimal slot/pole combinations FSCW IPM spoke type EPS motors. Two different low cost heavy rare earths free PM typologies, ferrite and hot-pressed NdFeB, are considered. A design and optimization procedure based upon the finite element analysis is presented. The impact of the magnetic properties and the slot/pole combination on the optimal motor dimensions, torque density, and motor cost is discussed. Cogging torque, torque ripple, electromechanical performance, and the stator deformation of the machines are evaluated, and the results are compared, highlighting the advantages and the differences among the solutions.**

***Index Terms*—AC motors, acoustic noise, brushless motors, electric machines, electric vehicles, electromagnetic forces, permanent magnet machines, power steering, rotating machines, vibrations.**

I. Introduction

IN AUTOMOTIVE applications, the research of high torque density, torque quality, and manufacturing simplicity for mass production emphasizes the fractional slot concentrated winding (FSCW) interior permanent magnet (IPM) synchronous motor as one of the most attractive candidates [1]–[5]. Among the IPM topologies, one of the most interesting is represented by the tangential magnetization or spoke type machine [6]–[11], reported in Fig. 1. Taking advantage of the flux concentration, spoke type motors provide the highest flux and torque density among the PM synchronous machines [12]. By means of the enhancing of the airgap flux density, the flux concentration yields to fully exploit heavy rare earths (HRE) free, low cost, and low remanence PM compounds such as ferrite or the recently introduced hot pressed NdFeB [13]–[15]. The interest in these PM compounds has grown in the recent years following the skyrocketing of the price of RE materials, such as Dysprosium (Dy) and Terbium (Tb). Recent research works proposed some novel rotor geometries such as a ferrite spoke-ring combination [16], a wing-shaped configuration [17], and a semimodular dual-stack rotor [18]. However, spoke type motors exhibit important drawbacks which are summarized in a limited flux weakening (FW) capability, lower saliency ratio (i.e., reluctance torque) [19]–[21], and lower demagnetization strength [7], [8], [12].

In [22]–[24], the influence of some design factors in a distributed winding spoke type motor has been investigated, considering different number of poles, magnet thickness, and shaft arrangement. In [25], an analytical procedure for FSCW IPM spoke type motor has been introduced in order to provide some design criteria aimed to PM volume minimization, considering different slot-pole arrangement. On the other hand, a detailed

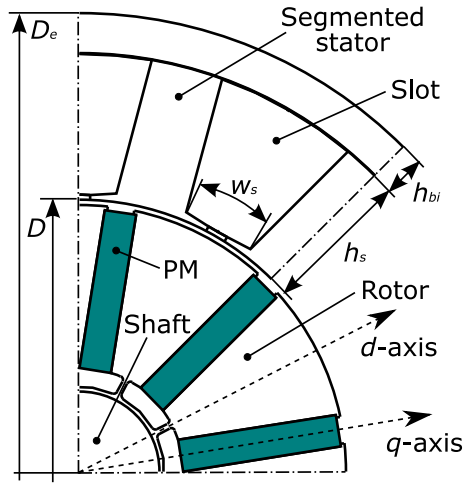

Fig. 1. 1/4 sketch of a spoke-type 12-slot 10-pole motor.

Manuscript received April 8, 2016; revised September 5, 2016 and March 11, 2017; accepted May 31, 2017. Date of publication February 18, 2018; date of current version May 18, 2018. Paper 2016-EMC-0169.R2, presented at the 2015 IEEE Energy Conversion Congress and Exposition, Montreal, QC, Canada, Sep. 20–24, and approved for publication in the IEEE TRANSACTIONS ON INDUSTRY APPLICATIONS by the Electric Machines Committee of the IEEE Industry Applications Society. *(Corresponding author: Enrico Carraro.)*

E. Carraro is with the Research and Development Department, SEG Automotive Germany GmbH, Stuttgart 70499, Germany (e-mail: enricocarraro85@gmail.com).

N. Bianchi is with the Department of Industrial Engineering, University of Padova, Padova 35122, Italy (e-mail: nicola.bianchi@unipd.it).

S. Zhang and M. Koch are with the Advanced Development Drives (DVE) Department, Brose Fahrzeugteile GmbH & Co. KG, Würzburg 97076, Germany (e-mail: sunny.zhang@brose.com; Matthias.Koch@brose.com).

Color versions of one or more of the figures in this paper are available online at http://ieeexplore.ieee.org.

Digital Object Identifier 10.1109/TIA.2018.2807382

analysis of the influence of the slot-pole combination on the motor performance, including torque quality, FW performance, and noise/vibration/harshness (NVH) has not been performed yet.

This paper aims to fill this gap [26]. It deals with the design and analysis of FSCW IPM spoke type motors for an electric power steering (EPS) application. In order to provide a comprehensive evaluation of the problem, eight promising slot/pole combinations, between 6 and 16 poles, have been selected. Two different HRE-free PM materials, a ferrite and a Dy-free hot-pressed NdFeB, have been considered for the rotor design. A design and optimization procedure based upon the finite element analysis (FEA) has been introduced. It is aimed at the maximization of the torque density and minimization of the cost. It allows a comprehensive investigation of the impact of the magnetic properties and the slot/pole combination on the optimal motor dimensions, torque density, and motor cost. Finally, the comparison of the electromechanical performance has been carried out, highlighting the advantages and drawbacks among the solutions.

II. Preliminary Analysis

A. Selection of the Optimal Slot/Pole Combinations

EPS systems require high performance in terms of torque density, torque quality, and NVH. Since these requirements are first influenced by the combination of the number of slots Q and poles $2{\cdot}p$, a preliminary selection of the most promising $Q/(2{\cdot}p)$ configurations has been carried out. The choice is based upon an evaluation of the following motor quality indexes:

1) high winding factor (main harmonic) k_{w1}, in order to improve the torque density;
2) high least common multiple $\mathrm{LCM}(Q, 2\cdot p)$, in order to reduce the cogging torque [3];
3) high and even great common divisor $(\mathrm{GCD})(Q, 2\cdot p)$ in order to reduce the unbalanced magnetic radial forces and increase the radial symmetry [3], [27].

As regards the number of poles, it is worth noticing that the flux concentration practically exists when the number of poles $2\cdot p \geq 6$ [6], [19], [25]. As the number of pole increases, the flux concentration become effective. On the other hand, an excessive increase of the number of poles does not yield a reduction of the PM volume for a given flux concentration ratio [25]. Even if a machine with a high number of poles $(2{\cdot}p > 16)$ can be theoretically designed, the higher supply frequency of the inverter and the higher manufacturing complexity cause these solutions to be not attractive for mass market production.

Based upon the previous argumentations, the most promising FSCW slot/pole candidates are evaluated and reported in Table I. Only the configurations with a number of slots per pole and phase $1/4 < q < 1/2$ have been considered since they exhibit a winding factor conveniently higher than 0.866. Finally, the selected configurations are $9/6$, $9/8$, $12/8$, $12/10$, $18/12$, $12/14$, $18/14$, and $18/16$. It is worth noticing that the combination with $\mathrm{GCD}(Q, 2\cdot p) = 1$, for, e.g., $9/8$ is usually avoided in automotive applications since it exhibit an asymmetric radial force distribution, hence a poor NVH behavior [28].

TABLE I
Comparison of the Motor Quality Indexes

$Q/(2{\cdot}p)$	q	k_{w1}	$\mathrm{LCM}(Q, 2{\cdot}p)$	$\mathrm{GCD}(Q, 2{\cdot}p)$
9/6	**1/2**	**0.866**	**18**	**3**
6/8	1/4	0.866	24	2
9/8	**3/8**	**0.945**	**72**	**1**
12/8	**1/2**	**0.866**	**24**	**4**
9/10	3/10	0.945	90	1
12/10	**2/5**	**0.933**	**60**	**2**
15/10	1/2	0.866	30	5
9/12	1/4	0.866	36	3
18/12	**1/2**	**0.866**	**36**	**6**
12/14	**2/7**	**0.933**	**84**	**2**
15/14	5/14	0.951	210	1
18/14	**3/7**	**0.902**	**126**	**2**
21/14	5/14	0.866	42	7
6/16	5/14	0.866	48	2
12/16	3/8	0.866	48	4
15/16	5/14	0.951	210	1
18/16	**5/14**	**0.945**	**144**	**2**
21/16	7/16	0.890	336	1
24/16	1/2	0.866	48	8

B. Rotor Design

One of the most intrinsic drawbacks of spoke type motors is the leakage flux, close to the shaft. For this reason, these machines are usually designed with a nonmagnetic shaft and joints between the rotor lamination and the shaft. Even if this rotor arrangement provides the best use of the magnet, it exhibit some drawbacks under the point of mass market production which are as follows.

1) Higher complexity of the manufacturing process because the rotor is not manufactured from a single mold.
2) The torque quality and NVH might be practically less controllable if the rotor lamination is not structurally a single piece (higher manufacturing tolerances).

For these reasons, a single rotor lamination equipped with an interlink inner bridge for each pole, has been considered in this analysis and it is reported in Fig. 1. In order to reduce the leakage flux, these bridges have to be designed to work in saturation.

III. Design and Optimization

The machines have been designed and optimized on the basis of the following constraints: outer diameter $D_e = 86$ mm, air-gap height $g = 0.5$ mm, shaft diameter $D_{ri} = 15$ mm, fill factor $k_{\mathrm{fill}} = 0.435$, and active copper losses $P_{\mathrm{Cua}} = 141$ W at 80 °C. The stack lengths L_{stk} have been adjusted in order to meet a 7.5 N·m rated torque target. The maximum speed is fixed to 2500 r/min. According to the inverter rating, a further constraint is given by the phase current $I_n \leq 100\ A_{\mathrm{RMS}}$ and dc bus fixed at 12 V. It follows that the number of conductors per each slot is defined and it has been selected for ensuring a double layer feasibility. The resistance of the converter and the dc bus has been taken into account.

The constraint of the fixed copper losses, assuming the iron losses to be negligible, ensures a comparable thermal behavior among the machines. Hence, for a given torque, i.e., stack length, the thermal losses density through the housing is constant. In order to have a comprehensive comparison, two

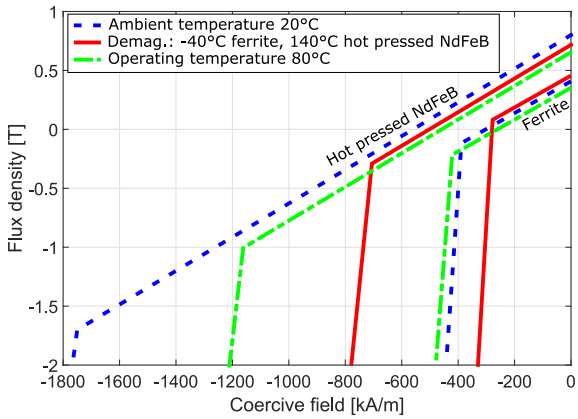

Fig. 2. Magnetization characteristic of the considered PMs.

different HRE-free PMs, a ferrite (grade 6) and a Dy-free hot-pressed NdFeB have been selected. Their B–H characteristic is reported in Fig. 2.

As shown in Fig. 1, the machine is equipped with a segmented stator [5]. This introduces an additional airgap but yields a high winding factor and easy winding process, especially in relation to the very limited overall motor dimensions. As a result of the segmented stator, for the mechanical feasibility, the slot opening is hybrid (sandwiched open and close slots). This configuration offers the advantage of comparable low cogging torque as for closed slot solutions without worsening the torque density in comparison to the open slot designs. It has been modeled considering an equivalent B–H curve, according to the method proposed in [29]. As reported in Fig. 1, the rotor ribs have been avoided in order to reduce the leakage flux.

The minimum thickness of the inner bridge has been preliminary evaluated on the basis of an analytical estimation, considering the worst case, taking into account the steady-state centrifugal pressure at the maximum speed and the magnetic pressure p_m.

A grade M330-50A iron lamination has been considered in this analysis. The estimated force acting on the inner bridge is

$$F_b = \frac{1}{n_b} \cdot \left(m_r \cdot R_m \cdot \Omega_{\text{MAX}}{}^2 + A_r \cdot p_m \right) \tag{1}$$

where $n_b = 2 \cdot p$ is the number of bridges, m_r is the estimated rotor mass, R_m is the average rotor diameter related to the position of the center of mass of the rotor iron, Ω_{MAX} is the maximum speed and A_r is the rotor outer surface, and p_m is the radial magnetic pressure. Such a parameter is assumed to be constant along the rotor periphery. Considering a homogenous rotor (PMs ad flux barriers have the same density of the iron) and assuming an average split ratio (airgap diameter D over D_e) $\delta = 0.6, p_m \cong 400$ kPa (equivalent to typical airgap flux density of about 1 T), the force on the bridge has been evaluated. Hence, the minimum thickness of the bridges has been computed by (2), assuming a safe factor $k_s = 3$

$$w_b = k_s \cdot \frac{F_b}{\sigma_y \cdot L_{\text{stk}}} \tag{2}$$

TABLE II
MINIMUM BRIDGE THICKNESS

9/6	9/8	12/8	12/10
0.114 mm	0.086 mm	0.086 mm	0.067 mm
18/12	12/14	18/14	18/16
0.057 mm	0.049 mm	0.049 mm	0.043 mm

where $\sigma_y = 354$ MPa is the iron yield stress and L_{stk} is the stack length. On the basis of the punching feasibility, the minimum thickness is 0.33 mm. This value is largely higher than those evaluated and reported in Table II, hence it has been selected for all the configurations.

A. Influence of the Motor Dimensions

An FE parametric analysis has been performed for each slot-pole combination in order to highlight the influence of the split ratio and stator cross-section to the torque density, airgap flux density, and active cost. The slot wedge and the opening height have been kept fixed. The slot opening width has been fixed to a 40% of the tooth width in order to keep the same aspect ratio during the calculation. As regards the PM cross-section, its length and width have been maximized in order to develop the highest airgap flux density, according to the rotor constraints [25]. The load simulation has been performed taking into account the actual current angle along the maximum torque per ampere locus. As mentioned before, with the constraint of the active copper losses, the slot current results

$$\widehat{I}_s = \sqrt{\frac{2 \cdot k_{\text{fill}} \cdot P_{Cua} \cdot S_s}{\rho_{Cu} \cdot Q \cdot L_{\text{stk}}}} \tag{3}$$

where ρ_{Cu} is the copper resistivity at 80 °C and S_s is the slot cross-section area.

Fig. 3 shows the torque density, the load airgap flux density map as a function of the split ratio δ, and slot width ratio w_{sr} (slot width w_s over the slot pitch) [30] evaluated by means of FEA. The back iron height ratio h_{bir} (back iron height h_{bi} over outer stator radius) has been evaluated in order to get the highest torque density. The used approach, of reporting the machine dimensions in relative terms instead of absolute quantities, yields to a generalization of the analysis and conclusions. It is worth noticing that, regardless the PM type, for a given slot/pole combination, each (δ, w_{sr}) point corresponds to the same stator, rotor, and PM cross-section. For each motor topology, an optimal split ratio, slot width, and back iron height ratio, which maximizes the torque, can be found. Due to the limited space in the paper, only the 12/10 machine is shown in detail in Fig. 3.

As reported in Fig. 3(a) and (b), the optimal split ratio is $\delta = 0.65$ and $\delta = 0.7$ with torque densities of 27.4 and 15.2 N·m/dm^3, respectively, for the MQ2 and the ferrite magnets. Regarding the slot width ratio, the ferrite design exhibits a higher value $w_{\text{sr}} = 0.61$ versus $w_{\text{sr}} = 0.51$. In fact a reduction of the tooth width in the ferrite solution is beneficial to the torque density since it can increase the slot current, without increasing the iron saturation. Both these behaviors are related to the lower airgap flux density achievable by such a PM. This is

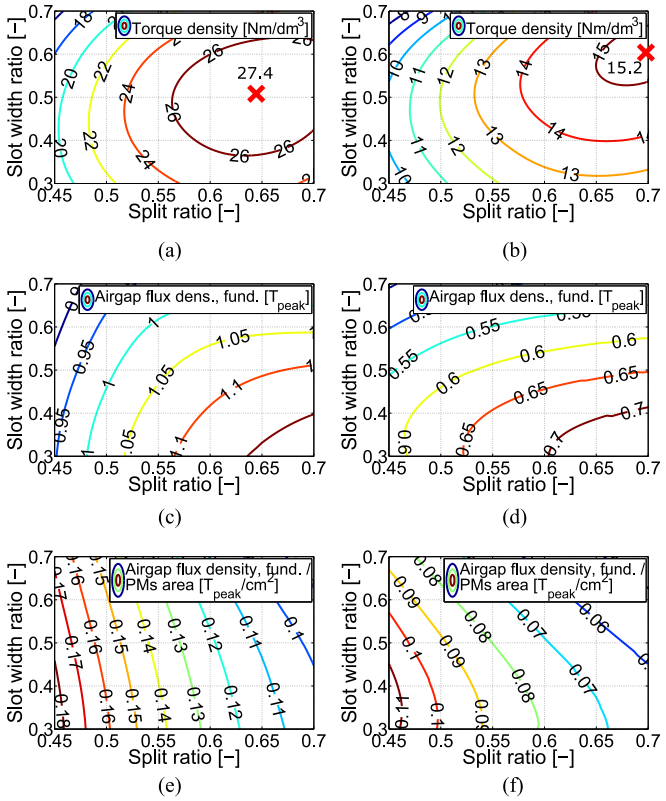

Fig. 3. 12-slot 10-pole motor: torque density and no load airgap flux density as a function of the main motor dimensions. (a) MQ2. (b) Ferrite. (c) MQ2. (d) Ferrite. (e) MQ2. (f) Ferrite.

shown in Fig. 3(c) and (d) which clearly highlights the increase of the flux concentration ratio as the split ratio increases. However, the airgap flux density per unit of PM area, reported in Fig. 3(e) and (f), shows that the lower the split ratio, the higher the effectiveness of the magnet.

An analysis of the costs provides interesting remarks. In Fig. 4, the active cost densities (active cost per unit of motor torque) are compared. The end winding cost, being a fixed contribution to the total cost, is neglected.

Since the MQ2 machine develops a torque density almost two times that of the ferrite machine, the active copper and iron cost densities are halved going from the ferrite to the MQ2. In Fig. 4(a) and (e), the active copper cost density increases going from higher to lower split ratio because the available slot area increases and the torque tends to decrease. The iron cost, instead, shows a global minimum for a slot width ratio $w_{\mathrm{sr}} = 0.6$ and split ratio $\delta = 0.6$.

Conversely, the PM cost density grows as the split ratio increases and this indicates the reduction of the effectiveness of the flux concentration effect when high split ratios are employed.

Finally, as highlighted in Fig. 4(d) and (h), a geometry with the minimum cost density exists and it can be different to that with the highest torque density. This is verified in the MQ2 motors, where the PM cost is almost four times the cumulative cost of the copper and iron, comparing to about one-third of the ferrite design. This emphasizes that in MQ2 machines, but in general when high cost magnets are used in spoke type configurations, the cheapest solutions can be found at low split ratios. Conversely, the ferrite solution is more effective since the geometry with the highest torque density is basically in the design area of the cheapest configurations. In conclusion for each $Q/(2\cdot p)$ combination, two representative solutions can be found: one with the highest torque density and one which shows the lowest cost. For all the considered slot/pole combinations, the above mentioned considerations result in having a general application. Since the lowest cost geometries are dependent on the actual costs of the active materials, the following analysis is focused to the highest torque density MQ2 solutions. Therefore, for the sake of the comparison, the slot opening width of each $Q/(2\cdot p)$ combination have been adjusted in order to reach the highest torque.

IV. Performance Comparison

In this section, the motor performance are compared and discussed. Fig. 5 reports the flux density maps at rated load of the final geometries. Table III reports the key machine dimensions and performance data.

Regarding the motor cross-section, all the slot/pole configurations show an optimal split ratio in a narrow range $\delta = 0.62 - 0.68$. The optimum split ratio increases with the number of poles and machines with the same number of poles exhibit basically the same split ratio.

Since the PM cross-section is different for each configuration, an evaluation of the no load airgap flux density provides an index of the effectiveness of the flux concentration. The results show that the flux concentration is less effective in the 6-pole machine, with a ratio equal to 0.104 $T_{\mathrm{peak}}/\mathrm{cm}^2$. Conversely, a global maximum is achieved in the 12-pole machine (0.130 $T_{\mathrm{peak}}/\mathrm{cm}^2$), while for a higher pole number such a ratio decreases [25].

A. Torque Density and Torque Quality Performance

Fig. 6 reports the comparison of the predicted torque density, cogging torque, and torque ripple for each $Q/(2\cdot p)$ combination.

The torque density is calculated by dividing the torque to the volume displaced by the stator $(1/4)\cdot\pi\cdot {D_e}^2\cdot L_{\mathrm{stk}}$. As shown in Fig. 6(a), the highest torque density, 30.38 N·m/dm^3 is achieved by $12/14$ configuration while the lowest, 21.18 N·m/dm^3 is exhibited by the $9/6$ machine. In general, these results confirm that the torque density in spoke type motors benefits from a high winding factor and flux concentration since, as mentioned in Section I and shown in Fig. 6(b), the reluctance torque contribution is negligible. However, the highest saliency ratio is found in the $9/6$ (1.906), $12/8$ (1.738), and $18/12$ (1.506) machines, which exhibit a number of slots per pole and phase is $q = 1/2$ [31]. Finally, in Table III, the total machine cost is reported. It is worth noticing that the cost follows, in an inverse law, the trend of the torque density. Hence, the $12/14$ machine results to be the cheapest.

Fig. 6(b) shows the comparison of the predicted cogging torque. The trend of the cogging torque as a function of the number of poles is basically in agreement with the cogging

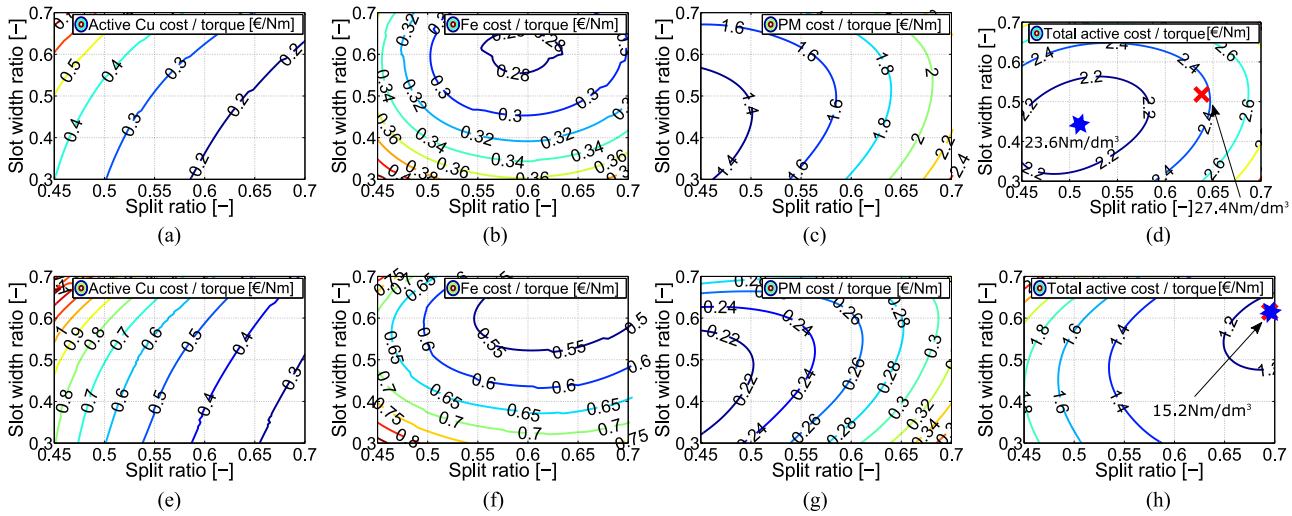

Fig. 4. 12-slot, 10-pole: active costs as a function of the main motor dimensions. (a) MQ2. (b) MQ2. (c) MQ2. (d) MQ2. (e) Ferrite. (f) Ferrite. (g) Ferrite. (h) Ferrite.

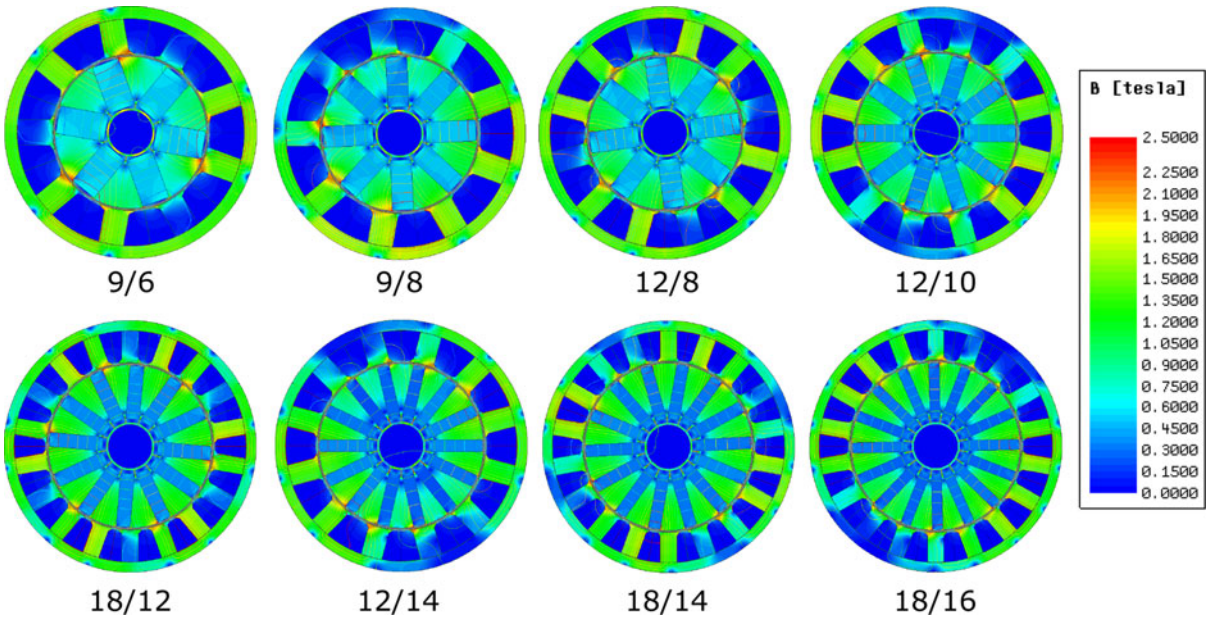

Fig. 5. MQ2 motors: flux density maps at rated load.

torque index highlighted in Section II. The $12/10$, $12/14$, $18/14$, and $18/16$ machines exhibit low cogging torque, in the range 25–100 mN·m (peak–peak). The lowest value is achieved by the $18/14$ motor.

As regards the torque ripple (under load), the predicted values are reported in Fig. 6(c). The trend is basically similar to that of the cogging torque, with low values in the range 2% achievable by $9/8$, $12/10$, $12/14$, $18/14$, and $18/16$ motors. The lowest torque ripple (1.77%) is predicted for the $18/14$ configuration.

B. Electromechanical Performance

The machine performance have been evaluated on the basis of the synchronous space vector control in the d/q reference frame. The iron losses are taken into account in the computation. However, for such an application, the copper losses are the dominant component in the whole speed range. Fig. 7(a), (b), and (c) reports torque, output power, and power factor versus speed, respectively. The best electromechanical characteristics are shown by the $12/14$ and $18/16$ machines, while the lowest speed range is exhibited by the $9/6$ configuration. It is worth noticing that the FW range can be improved for all the machines with a different selection of the machine geometry.

Further analysis have been performed in order to verify the demagnetization at the worst operating condition in FW operation. The machines have been fed with a demagnetization current (d-axis) at the test temperature 140 °C. The PM demagnetization distribution has been frozen and a no load analysis

TABLE III
MACHINE PARAMETERS COMPARISON

	9/6	9/8	12/8	12/10	18/12	12/14	18/14	18/16	Unit
Stack length	61	49	54.5	47	51	42.5	48.5	46	mm
Split ratio	0.62	0.63	0.62	0.65	0.66	0.67	0.68	0.68	–
Slot width ratio	0.56	0.56	0.51	0.51	0.45	0.54	0.47	0.48	–
Back iron ratio	0.1	0.1	0.09	0.09	0.083	0.085	0.08	0.076	–
Slot current	1265	1230	931	887	559	878	551	553	A_{peak}
# of cond./slot, equiv. series	10	10	7	7	4	7	4	4	–
Current density	12.3	12.6	12.7	13.2	14.1	13.5	14.2	14.1	A/mm^2
Electric loading	59.3	61.4	57.7	57.0	48.8	54.7	49.0	51.1	$kA_{\text{peak}}/\text{m}$
No load flux dens., fun.	0.98	1.10	1.15	1.22	1.33	1.22	1.33	1.31	T_{peak}
No load flux dens., fun./PMs area	0.104	0.113	0.122	0.123	0.130	0.120	0.127	0.125	$T_{\text{peak}}/\text{cm}^2$
Saliency ratio (@ base point)	1.906	1.174	1.738	1.240	1.506	1	1.177	1.070	–
Torque density	21.18	26.35	23.64	27.46	25.31	30.38	26.57	27.00	$\text{N}\cdot\text{m}/\text{dm}^3$
Cogging torque peak-peak	1218	146	1100	93.3	1591	75.6	25.0	76.7	mN·m
Torque ripple	22.0	2.56	11.9	2.72	13.7	2.85	1.77	2.86	%
Max deform. (@ base point, 1000 r/min)	0.51	0.78	0.47	0.40	0.12	0.48	0.31	0.32	μm
Total cost	23.41	19.25	20.74	18.55	20.13	17.13	19.45	18.50	€

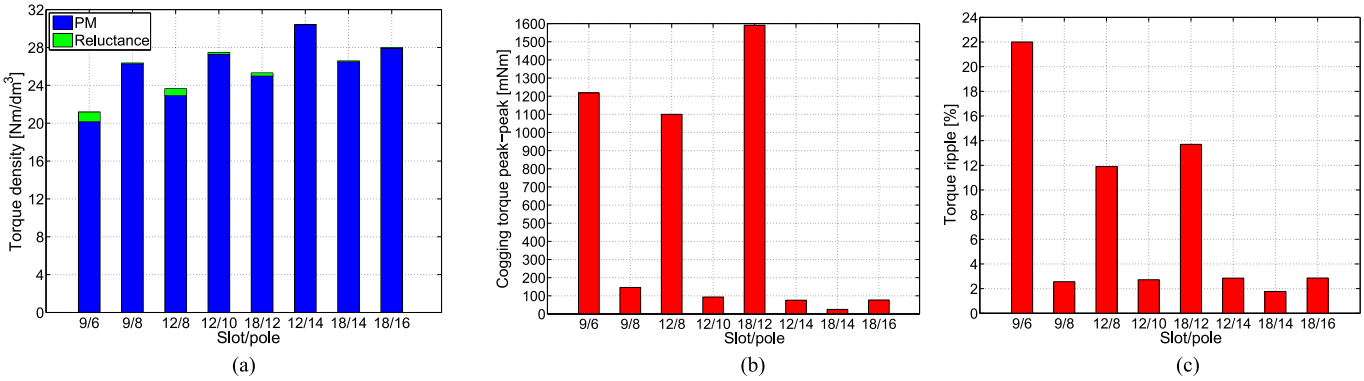

Fig. 6. Torque density, cogging torque, and torque ripple for each slot/pole combination. (a) Torque density. (b) Cogging torque. (c) Torque ripple.

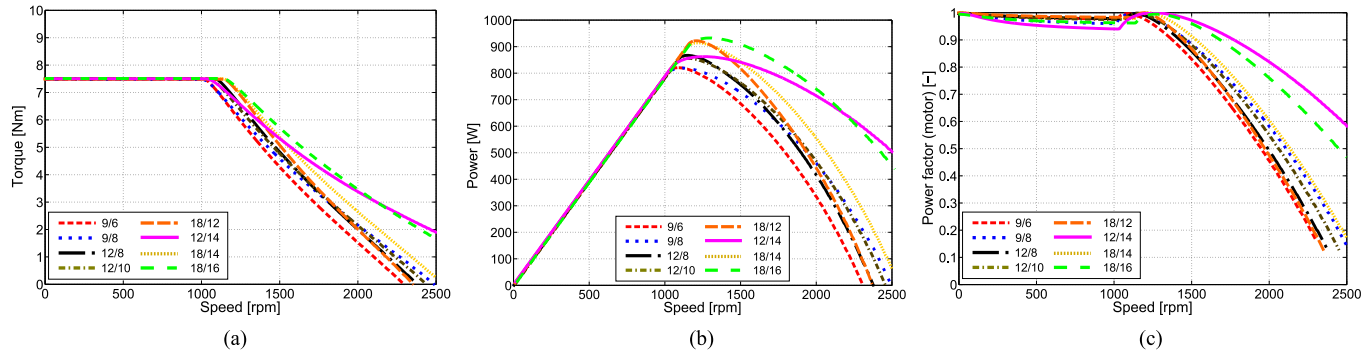

Fig. 7. Electromechanical performance. (a) Torque versus speed. (b) Power versus speed. (c) Power factor versus speed.

has been subsequently performed showing a negligible reduction of the PM flux linkage. Finally, an FEA structural analysis has been carried out on each rotor, at the maximum speed. It confirms the structural integrity of the selected geometries.

C. Stator Deformation Analysis

The acoustic behavior of PM machines is a complex issue, since it involves magnetic, mechanical (assembly and bearing), and aerodynamic (cooling flow) sources. In the present section, the magnetic source is studied.

The radial deformations of the stator structure due to the magnetic forces acting on the inner surface, namely the tooth tips and the hybrid slot openings, are the main cause of the magnetic noise in PM machines [28], [32]. Tangential forces can be considered negligible for the noise and vibration phenomena being usually negligible in comparison to the radial component [33]. In Fig. 8, the airgap radial pressure plot as a function

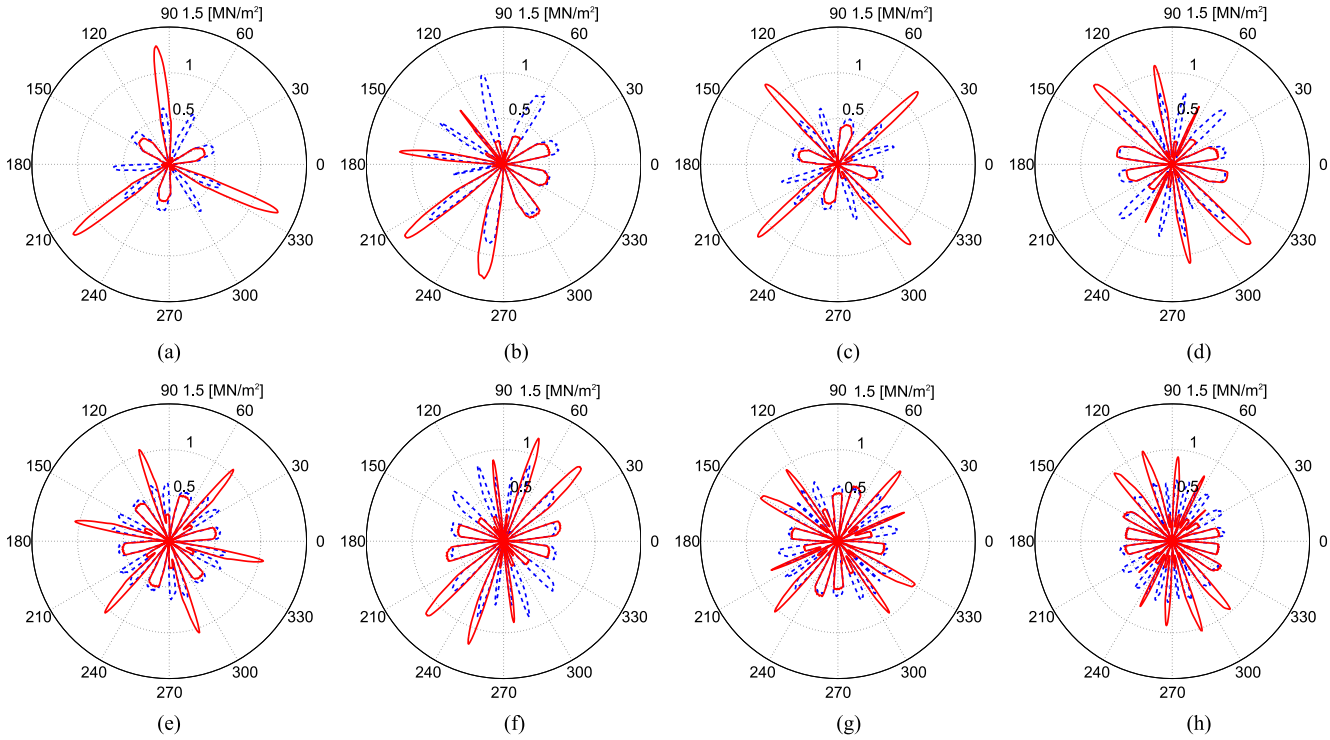

Fig. 8. Polar plot of the airgap radial pressure in rated load (red line) and no load (blue dashed line) operation. (a) 9/6. (b) 9/8. (c) 12/8. (d) 12/10. (e) 18/12. (f) 12/14. (g) 18/14. (h) 18/16.

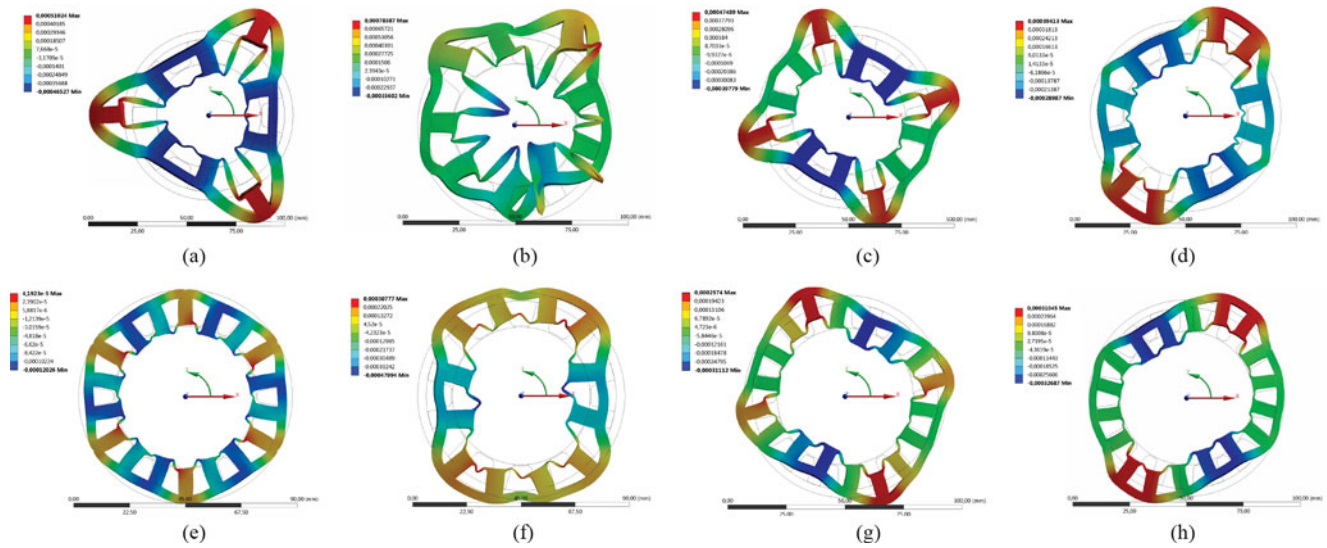

Fig. 9. MQ2 motors: radial deformation at the rated torque and 1000 r/min ($2.5 \cdot 10^4$ magnification factor). (a) 9/6. (b) 9/8. (c) 12/8. (d) 12/10. (e) 18/12. (f) 12/14. (g) 18/14. (h) 18/16.

of the angular position is reported. Each slot-pole combination shows a specific pattern related to the GCD$(Q, 2 \cdot p)$, reported in Table I. While the loading condition does not influence the periodicity of this pattern, its amplitude is clearly affected. As the rotor is rotating, this space distribution rotates maintaining the similar shape, acting on the stator structure, and producing deformation.

The stator deformation of the different $Q/(2 \cdot p)$ machines have been computed by means of a coupled magnetic and structural analysis. The machines have been analyzed at the base point (7.5 N·m) and speed 1000 r/min. The total magnetic forces acting on the inner stator surface have been computed and their harmonic content evaluated. This quantity has been then used as a mechanical load in a structural FEA of the stator. All the

machines share the same boundary condition represented by six equispaced fixed support along the stator periphery. Fig. 9 shows the predicted radial deformation for each slot/pole combination. It has been proved that the shape of the stator deformation is in correlation with the space distribution of the magnetic force acting on the inner stator surface [34]. This shape is related to the pattern of the airgap radial pressure distribution reported in Fig 8. The deformation comes mainly from the excitement of a specific vibration mode, represented by the following orders:

1) 1 for the $9/8$, 3 for the $9/6$;
2) 2 for the $12/10$, $12/14$, $18/14$, $18/16$;
3) 4 for the $12/8$;
4) 6 for the $18/12$ machine.

As the displacement is proportional to the fourth power of the mode order [34], the lower the dominant vibration mode, the higher the stator deformation.

The maximum radial deformation, reported in Table III, confirms this theoretical approach. For the sake of simplicity, four different $Q/(2 \cdot p)$ classes can be highlighted. The first, with the highest deformation, 0.78 μm is represented by the $9/8$ machine. This configuration, as discussed before, is well known to exhibit high NVH issues, since it is characterized by an unbalanced magnetic pull. The second class, represented by the $9/6$, $12/8$, $12/10$, and $12/14$ machines, shows displacements in the range 0.40–0.51 μm. Lower deformation is placed in the third class, represented by the $18/14$ and $18/16$ machines, with values in the range of 0.30–0.32 μm. Finally, the lowest amplitude is shown in the last class, the $18/12$ machine, with a maximum radial deformation of 0.13 μm, about 70% lower than the second class. However, even though this last combination results to be potentially attractive for an excellent NVH behavior, on the other hand, it exhibits high levels of torque ripple and cogging torque.

V. Conclusion

This paper investigates the influence of slot/pole combination on the performance of an FSCW IPM spoke type motor. On the basis of a preliminary evaluation of the main motor quality indexes, eight optimal configuration in the range between 6 and 16 poles have been selected and investigated.

On the basis of geometrical and electrical constraints, the influence of the geometrical dimension on the torque density and cost has been studied, comparing two different HRE-free PM solutions, a hot-pressed NdFeB and a ferrite magnet. Due to the different weights of the cost materials (copper, iron, PMs) and the different cost functions as regards to the motor dimensions, the optimum solution for the cost and the optimum solution for the torque can be found in similar or different design areas. Although low cost and low remanence magnet solutions, such as with ferrite, are not able to achieve high torque density, they are more effective in a spoke type structure because they develop the highest torque density at the lowest cost. Conversely, in high cost and high remanence magnet machines, the cheapest solution is not equivalent to the highest torque density configuration.

It has been shown that machines with low pole number (6-and 8-pole) develop lower torque density than those with higher pole number.

Finally, torque quality, electromechanical performance have been finally evaluated and compared among the different slot/pole combinations. An analysis of the stator core displacement, due to magnetic forces, has been carried out in order to provide an assessment of the NVH issue. It has been proved that the NVH is strictly dependent on the selected slot/pole combination and is generally independent on the torque quality performance. For instance, the best acoustic performance are shown by the machines with the high periodicity, such as the $18/12$ configuration. On the other hand, this latter design exhibits the lowest torque quality. In conclusion, there is no slot/pole combination fulfilling the best performance targets at the same time. On the other hand, this research shows that, among the selected slot/pole combinations, the solution with high number of poles exhibit higher overall performance in terms of torque density, torque quality, FW performance, and NV. Among them, the 12-slot 14-pole shows the best performance, with the highest torque density and lowest cost, thus representing an ideal slot/pole combination in spoke type motors for mass market production.

Acknowledgment

The authors would like to thank Brose Fahrzeugteile GmbH & Co. KG, Würzburg, Germany, for supporting this project.

References

[1] N. Bianchi, "Permanent magnet synchronous motors," in *Industrial Electronics Handbooks, Power Electronics and Motor Drives*, 2nd ed. Boca Raton, FL, USA: CRC Press, 2011, pp. 6.1–6.35.

[2] F. Magnussen and C. Sadarangani, "Winding factors and joule losses of permanent magnet machines with concentrated windings," in *Proc. IEEE Int. Elect. Mach. Drives Conf.*, 2003, vol. 1, pp. 333–339.

[3] A. EL-Refaie and T. Jahns, "Optimal flux weakening in surface PM machines using fractional-slot concentrated windings," *IEEE Trans. Ind. Appl.*, vol. 41, no. 3, pp. 790–800, May/Jun. 2005.

[4] B. Mecrow *et al.*, "Design and testing of a four-phase fault-tolerant permanent-magnet machine for an engine fuel pump," *IEEE Trans. Energy Convers.*, vol. 19, no. 4, pp. 671–678, Dec. 2004.

[5] A. El-Refaie, "Fractional-slot concentrated-windings synchronous permanent magnet machines: Opportunities and challenges," *IEEE Trans. Ind. Electron.*, vol. 57, no. 1, pp. 107–121, Jan. 2010.

[6] US Department of Energy, "Final report on assessment of motor technologies for traction drives of hybrid and electric vehicles," 2011. [Online]. Available: http://info.ornl.gov/sites/publications/files/pub28840.pdf

[7] G.-H. Kang, J. Hur, H.-G. Sung, and J.-P. Hong, "Optimal design of spoke type BLDC motor considering irreversible demagnetization of permanent magnet," in *Proc. 6th Int. Conf. Elect. Mach. Syst.*, 2003, vol. 1, pp. 234–237.

[8] B. kuk Lee, G.-H. Kang, J. Hur, and D.-W. You, "Design of spoke type BLDC motors with high power density for traction applications," in *Proc. 39th IAS Annu. Meeting—Conf. Rec. IEEE Ind. Appl. Conf.*, 2004, vol. 2, pp. 1068–1074.

[9] Y. Demir, O. Ocak, and M. Aydin, "Design, optimization and manufacturing of a spoke type interior permanent magnet synchronous motor for low voltage-high current servo applications," in *Proc. IEEE Int. Elect. Mach. Drives Conf.*, May 2013, pp. 9–14.

[10] E. Sulaiman, T. Kosaka, and N. Matsui, "Design optimization of 12 slot-10 pole hybrid excitation flux switching synchronous machine with 0.4 kg permanent magnet for hybrid electric vehicles," in *Proc. IEEE 8th Int. Conf. Power Electron. ECCE Asia*, May 2011, pp. 1913–1920.

[11] P. Zhang, G. Sizov, D. Ionel, and N. Demerdash, "Establishing the relative merits of interior and spoke-type permanent magnet machines with ferrite or ndfeb through systematic design optimization," *IEEE Trans. Ind. Appl.*, vol. 51, no. 4, pp. 2940–2948, Jul./Aug. 2015.

[12] A. Fasolo, L. Alberti, and N. Bianchi, "Performance comparison between switching-flux and IPM machine with rare earth and ferrite PMs," in *Proc. 20th Int. Conf. Elect. Mach.*, 2012, pp. 731–737.

[13] R. Lee, E. Brewer, and N. Schaffel, "Processing of neodymium-iron-boron melt-spun ribbons to fully dense magnets," *IEEE Trans. Magn.*, vol. 21, no. 5, pp. 1958–1963, Sep. 1985.
[14] Molycorp Magnequench, "Rare earth hot pressed permanent magnets application guide mq2," [Online]. Available: www.mqitechnology.com/downloads/articles/MQ2-Application-Guides-2012–10-23.p
[15] S. Zhang *et al.*, "Permanent magnet technology for electric motors in automotive applications," in *Proc. 2nd Int. Elect. Drives Prod. Conf.*, 2012, pp. 1–11.
[16] M. Rahman, K.-T. Kim, and J. Hur, "Design and analysis of a spoke type motor with segmented pushing permanent magnet for concentrating air-gap flux density," *IEEE Trans. Magn.*, vol. 49, no. 5, pp. 2397–2400, May 2013.
[17] M. Rahman, K.-T. Kim, and J. Hur, "Design and optimization of neodymium-free SPOKE-type motor with segmented wing-shaped PM," *IEEE Trans. Magn.*, vol. 50, no. 2, pp. 865–868, Feb. 2014.
[18] S. Sashidhar and B. Fernandes, "A low-cost semi-modular dual-stack PM BLDC motor for a PV based bore-well submersible pump," in *Proc. Int. Conf. Elect. Mach.*, Sep. 2014, pp. 24–30.
[19] N. Bianchi and T. Jahns, *Design, Analysis, and Control of Interior PM Synchronous Machines*. Padova, Italy: CLEUP, 2004.
[20] S.-O. Kwon, S.-I. Kim, P. Zhang, and J.-P. Hong, "Performance comparison of ipmsm with distributed and concentrated windings," in *Proc. 41st IAS Annu. Meeting—Conf. Rec. IEEE Ind. Appl. Conf.*, 2006, vol. 4, pp. 1984–1988.
[21] F. Charih, F. Dubas, C. Espanet, and D. Chamagne, "Performances comparison of pm machines with different rotor topologies and similar slot and pole numbers," in *Proc. Int. Symp. Power Electron. Elect. Drives Autom. Motion*, Jun. 2012, pp. 56–59.
[22] C. Zhao, S. Li, and Y. Yan, "Influence factor analysis of PMSM air gap flux density," in *Proc. Eighth Int. Conf. Elect. Mach. Syst.*, Sep. 2005, vol. 1, pp. 334–339.
[23] C. Zhao, H. Haihong, Qin, and Y. Yan, "Analysis of the pole numbers on flux and power density of IPM synchronous machine," in *Proc. Int. Conf. Power Electron. Drives Syst.*, 2005, vol. 2, pp. 1402–1407.
[24] A. Sorgdrager and A. Grobler, "Influence of magnet size and rotor topology on the air-gap flux density of a radial flux PMSM," in *Proc. IEEE Int. Conf. Ind. Technol.*, Feb. 2013, pp. 337–343.
[25] E. Carraro, N. Bianchi, S. Zhang, and M. Koch, "Permanent magnet volume minimization of spoke type fractional slot synchronous motors," in *Proc. IEEE Energy Convers. Congr. Expo.*, Sep. 2014, pp. 4180–4187.
[26] E. Carraro, N. Bianchi, S. Zhang, and M. Koch, "Performance comparison of fractional slot concentrated winding spoke type synchronous motors with different slot-pole combinations," in *Proc. IEEE Energy Convers. Congr. Expo.*, Sep. 2015, pp. 6067–6074.
[27] F. Magnussen and H. Lendenmann, "Parasitic effects in PM machines with concentrated windings," *IEEE Trans. Ind. Appl.*, vol. 43, no. 5, pp. 1223–1232, Sep./Oct. 2007.
[28] R. Islam and I. Husain, "Analytical model for predicting noise and vibration in permanent-magnet synchronous motors," *IEEE Trans. Ind. Appl.*, vol. 46, no. 6, pp. 2346–2354, Nov. 2010.
[29] Z. Azar, Z. Zhu, and G. Ombach, "Investigation of torque-speed characteristics and cogging torque of fractional-slot IPM brushless ac machines having alternate slot openings," *IEEE Trans. Ind. Appl.*, vol. 48, no. 3, pp. 903–912, May 2012.
[30] W. Soong, "PM synchronous machine modelling and design," in *Proc. IEEE Energy Convers. Congr. Expo.*, 2014, pp. 59–75.
[31] J. Tangudu, T. Jahns, and A. El-Refaie, "Unsaturated and saturated saliency trends in fractional-slot concentrated-winding interior permanent magnet machines," in *Proc. IEEE Energy Convers. Congr. Expo.*, Sep. 2010, pp. 1082–1089.
[32] J. Gieras, C. Wang, C. Joseph, and N. Ertugrul, "Analytical prediction of noise of magnetic origin produced by permanent magnet brushless motors," in *Proc. Elect. Mach. Drives Conf.*, May 2007, vol. 1, pp. 148–152.
[33] D. Fodorean, M. Sarrazin, C. Martis, J. Anthonis, and H. Van der Auweraer, "Characterizing the motorization of a light electric vehicle through FEM and NVH tests," in *Proc. Int. Conf. Elect. Mach.*, Sep. 2014, pp. 2404–2409.
[34] M. Islam, R. Islam, and T. Sebastian, "Noise and vibration characteristics of permanent-magnet synchronous motors using electromagnetic and structural analyses," *IEEE Trans. Ind. Appl.*, vol. 50, no. 5, pp. 3214–3222, Sep. 2014.

Enrico Carraro received the B.S., M.S., and Ph.D. degrees in electrical engineering from the University of Padova, Padova, Italy, in 2007, 2012, and 2017, respectively.

From 2013 to 2016, he was a Ph.D. student in the Electric Drives Laboratory, Department of Industrial Engineering, University of Padova, working in collaboration with Brose Fahrzeugteile GmbH & Co. KG, Wrzburg, Germany. Since 2017, he has been with Robert Bosch Starter Motors Generators Holding GmbH (SEG Automotive Germany GmbH), Stuttgart, Germany, since 2018. His research activities include the design and analysis of permanent magnet synchronous machines for hybrid and all-electric vehicles.

Nicola Bianchi (M'98–SM'09–F'14) received the M.Sc. and Ph.D. degrees in electrical engineering from the University of Padova, Padova, Italy, in 1991 and 1995, respectively.

In 1998, he joined the Department of Electrical Engineering, University of Padova, as an Assistant Professor. Since 2005, he has been an Associate Professor of electrical machines, converters, and drives with the Electric Drive Laboratory, Department of Electrical Engineering, University of Padova. His teaching activity deals with the design methods of electrical machines, where he introduced the finite-element analysis of machines. He is the author or co-author of several scientific papers and international books on electrical machines and drives. His research interests include the field of design of electrical machines, particularly for drive applications, in which he is responsible for various projects for local and foreign industries.

Dr. Bianchi is a member of the Electric Machines Committee and the Electrical Drives Committee of the IEEE Industry Applications Society. He is the recipient of five awards for best conference and journal papers. He served as Technical Program Chair for the 2014 IEEE Energy Conversion Congress and Exposition and is an Associate Editor for the IEEE TRANSACTION ON INDUSTRY APPLICATIONS and *IET-EPA Proceedings*.

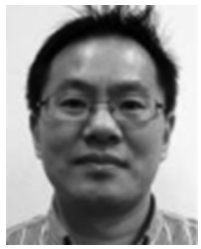

Sunny Zhang received the technical doctor degree in applied electromagnetics from the Lulea University of Technology, Luleå, Sweden, in 1999.

From 1999 to 2010, he worked for Bakker Magnetics, Eindhoven, The Netherlands, as a Research and Development Manager. From 2010 to 2011, he worked for the Wijdeven Group, Oirschot, The Netherlands, as the Chief Technical Officer, responsible for long-stroke and short-stroke magnetic actuators development for semiconductor industry and other types of magnetic motion systems. Since 2012, he has been with Brose Fahrzeugteile GmbH, Wrzburg, Germany, as a Senior Expert for magnet and motor technology development. He holds more than 12 international patents for various magnetics applications.

Matthias Koch was born in Germany on January 25th, 1979. He received the graduate degree in mechanical engineering with central focus on mechatronics, and the Dipl-Ing. degree in mechanical engineering dealing with control and mechanical design of an automotive actuator from the University of Paderbom, Paderborn, Germany, in 2005.

From 2005 to 2008, he was at Siemens VDO as a Calculation Engineer for electromechanical systems, including multiphysical approaches in acoustics of electrical motors. Until 2011, he continued his work as a Calculation Engineer for new smart motor designs at Brose Fahrzeugteile GmbH & Co. KG, Würzburg, Germany. Since the summer of 2011, he has been the Head of the Electric Drives Simulation Group which is working in fields of developing and designing innovative brushless ac and dc motors.